NASA TM X-309

TECHNICAL MEMORANDUM

X-309

FREE-FLIGHT MEASUREMENTS OF THE BASE PRESSURES AND DRAG OF A FLARE-STABILIZED CYLINDRICAL REENTRY BODY WITH AN ELLIPTICAL BLUNT NOSE AT MACH NUMBERS FROM 1.9 TO 0.7

By Robert J. Mayhue

Langley Research Center
Langley Field, Va.

NATIONAL AERONAUTICS AND SPACE ADMINISTRATION
WASHINGTON
September 1960

NATIONAL AERONAUTICS AND SPACE ADMINISTRATION

TECHNICAL MEMORANDUM X-309

FREE-FLIGHT MEASUREMENTS OF THE BASE PRESSURES AND DRAG OF A FLARE-STABILIZED CYLINDRICAL REENTRY BODY WITH AN ELLIPTICAL BLUNT NOSE AT MACH NUMBERS FROM 1.9 TO 0.7*

By Robert J. Mayhue

SUMMARY

A free-flight test was conducted to determine the base pressures and drag of a flare-stabilized reentry body during a descending trajectory over a Mach number range from 1.9 to 0.7 and a Reynolds number range from 4.75×10^6 to 2.62×10^6. The model was tested with the center of gravity located at 42.7 percent of the body length. The reentry body configuration consisted of a cylindrical center section, a 16.5° half-angle flare afterbody for stabilization, and an elliptical blunt nose with a ratio of nose length to body radius of 0.29. The overall fineness ratio of the model was 3.15.

High-amplitude oscillations were experienced by the decelerating model at the transonic and subsonic speeds and resulted in a large spread in the measured values of the axial-force and base pressure coefficients below Mach number 1.25. A region of dynamic instability was indicated by divergent oscillations of the model at the transonic speeds. Comparison of the drag coefficients of the present model with those obtained from free-flight tests of similar models showed fairly good agreement as the oscillating models approached zero angle of attack at supersonic speeds. Comparison of the present results with the results of free-flight tests of similar models with a less blunt nose indicated that a decrease in the ratio of nose length to body radius from 0.50 to 0.29 resulted in an increase in the total drag coefficient at approximately zero angle of attack of about 0.2 at supersonic speeds. The effect of nose bluntness on the base drag coefficients at approximately zero angle of attack appeared to be negligible at Mach numbers above 1.25.

*Title, Unclassified.

INTRODUCTION

A free-flight test program has been conducted by the Langley Research Center to determine the performance characteristics of reentry bodies consisting of blunt-nose cylinders with flared afterbodies for stabilization. Base pressures and drag measurements at Mach numbers from 0.7 to 1.9 are presented in reference 1 for a cylindrical reentry body having a 16.5° half-angle flare and an elliptical blunt nose with a ratio of nose length to body radius of 0.50. References 2 and 3 present drag and pressure measurements for a similar reentry body configuration except that the configuration had a blunter nose with a ratio of nose length to body radius of 0.29. These tests were conducted at Mach numbers from 4.3 to 0.6.

The foregoing tests showed that the average drag and base pressures measured during decelerating flight were dependent on the amplitude of the oscillations experienced by the models at the transonic and subsonic speeds. The range of the base pressures as the result of the high-amplitude oscillations of the configuration becomes an important factor in cases where accurate operation of base-pressure actuated switches is desired. The purpose of the present paper is to obtain drag and base pressure measurements on a model whose flight path was programed to simulate the decelerating forces of a full-scale missile during the terminal phase of reentry. The model was similar to that of reference 1 but with the nose bluntness ratio of the present model reduced from 0.50 to 0.29 in an effort to obtain some of the effects of nose bluntness on the base pressures and drag of the decelerating model. The test was conducted at the NASA Wallops Station and covered a Reynolds number range, based on the body diameter, from 4.75×10^6 (at Mach number 1.9) to 2.62×10^6 (at Mach number 0.7).

SYMBOLS

A	reference area (cross-sectional area of cylindrical body), 0.442 sq ft
A_b	base area, 0.961 sq ft
a_l	longitudinal accelerometer reading, g units
a_n	normal accelerometer reading, g units

a_t transverse accelerometer reading, g units

C_A axial-force coefficient, $-a_l \frac{W}{qA}$

$C_{D,b}$ base drag coefficient obtained from base pressure measurements, $\overline{C}_p \frac{A_b}{A}$

$C_{D,t}$ total drag coefficient (based on reference area of 0.442 sq ft) $C_A \cos \alpha + C_R \sin \alpha$

C_N normal-force coefficient, $a_n \frac{W}{qA}$

C_p base pressure coefficient, $\frac{p_b - p_\infty}{q}$

$\overline{C}_p$ average base pressure coefficient

C_R resultant-force coefficient, $\sqrt{C_N^2 + C_Y^2}$

C_Y transverse-force coefficient, $a_t \frac{W}{qA}$

I_X, I_Y, I_Z moments of inertia about X-, Y-, and Z-axes, respectively, slug-ft^2

l nose length measured to point of tangency with cylindrical center section, in. (fig. 1)

M free-stream Mach number

P base-pressure orifice

p_b base pressure, lb/sq ft unless otherwise specified

p_t total pressure, lb/sq ft unless otherwise specified

p_∞ free-stream static pressure, lb/sq ft unless otherwise specified

q free-stream dynamic pressure, lb/sq ft

R	free-stream Reynolds number, based on diameter of cylindrical body
r	radius of cylindrical body, in.
t	time, sec
W	weight, lb
x,y	nose coordinates
x',y'	backplate coordinates
α	resultant angle of attack, angle between model longitudinal axis and flight path, deg
$\dot{\theta}$	angular velocity in pitch, radians/sec
$\dot{\psi}$	angular velocity in yaw, radians/sec

Subscripts:

1	station 1
m	manifold

MODELS AND BOOSTERS

The external shape and general dimensions of the model are presented in figure 1 and a photograph is presented in figure 2. The model was constructed of stainless steel and consisted of an elliptical blunt nose, a cylindrical center section, and a 16.5° cone-frustum afterbody made of fiber glass. The nose of the model had a ratio of nose length to body radius of 0.29 and the shape of the nose is defined by the coordinates as given in figure 1. The base of the afterbody was covered with a backplate having a spherical curvature defined by the coordinates listed in figure 1. Dummy fixtures were attached to the base of the model to simulate reentry attitude controls. The model had an overall fineness ratio of 3.15. The mass characteristics of the model are as follows:

Weight, lb	205
I_Y or I_Z, slug-ft^2	4.59
I_X, slug-ft^2	0.63
Center of gravity, percent body length	42.7

A photograph showing the model and booster system in the launching position is shown in figure 3. The booster system consisted of a fin-stabilized, solid-propellant Nike rocket motor for the first-stage booster and a fin-flare-stabilized, solid-propellant Cajun rocket motor as the second-stage booster. The second-stage flare had a 20° half-angle and provided additional drag for separation of the model at burnout of the Cajun booster.

INSTRUMENTATION

A telemeter was carried in the model and continuously transmitted measurements of the normal, transverse, and longitudinal accelerations, total pressure at the nose, base pressures, rate of pitch, and rate of yaw. The locations of the base pressure orifices are shown in figure 4. Ground instrumentation included a CW Doppler radar unit to measure velocity of the model and an NASA modified SCR-584 tracking radar to determine the flight path. Atmospheric data were obtained from a rawinsonde released from the ground immediately before launching of the model.

FLIGHT TEST AND DATA REDUCTION

The model was launched at an angle of 75° from the horizontal and was accelerated to a maximum Mach number of approximately 2.4 by the first-stage Nike booster. The Nike booster separated at burnout, and the model and second-stage Cajun booster coasted up and over the top of a ballistic trajectory as shown in figure 5(a). The second-stage Cajun booster was ignited shortly after apogee and accelerated the model to a maximum Mach number of approximately 2.0. The model and second-stage booster separated shortly after burnout of the booster.

Both CW Doppler and SCR-584 radar lost contact with the model shortly after separation of the model from the second-stage Cajun booster. The data portion of the descending trajectory (after separation of the model) was computed step by step from telemeter measurements of the model deceleration and total pressures at the nose. Comparison of the velocities computed from the model deceleration and from the total pressures at a given time and altitude showed good agreement. Cumulative trajectory errors should be negligible since a large part of the data portion of the trajectory from Mach numbers 1.9 to 1.0 was covered in only a 3,200-foot altitude change.

The Reynolds number during the data portion of the reentry trajectory varied from 4.75×10^6 to 2.62×10^6 (based on body diameter)

at Mach numbers 1.9 and 0.7, respectively, The variation of Reynolds number with Mach number is presented in figure 5(b). The time histories of the dynamic pressure and Mach number are presented in figure 6 for the data portion of the test. The measured accelerations and base pressures were reduced to coefficient form as indicated in the section entitled "Symbols."

Approximate resultant angles of attack of the model were estimated from cross plots of normal-force coefficients against angle of attack obtained from unpublished wind-tunnel tests of similar models. Resultant angles of attack greater than 18° were obtained by extrapolation of the wind-tunnel results.

Estimated maximum experimental errors are based on an instrument error of ±2 percent of the full-scale instrument range. The total pressure is estimated to be accurate within ±2.33 lb/sq in.; the base pressure, within ±0.28 lb/sq in.; and the free-stream static pressure, within ±0.11 lb/sq in. The estimated accuracy for the aerodynamic coefficients for the model at several representative Mach numbers is

Coefficient	Accuracy at Mach number -		
	1.86	1.20	0.70
C_A	±0.12	±0.27	±0.41
C_N	±0.10	±0.22	±0.33
C_Y	±0.10	±0.22	±0.33

The Mach number is estimated to be accurate within ±2 percent over the range of Mach numbers indicated. Based on the scatter of data points, the random errors are believed to be much smaller than the magnitude of the errors stated.

DISCUSSION OF RESULTS

Model Motions

An indication of the motions of the model during the data portion of the reentry trajectory is given in the plots of the variation of the normal-force coefficient with the transverse-force coefficient in figure 7 and in the time history of the square of the resultant-force coefficients in figure 8. Oscillations of the model began at a Mach number of 1.25 after a buildup in the resultant angle of attack to approximately 16°. While the model decelerated through a region of

dynamic instability as indicated by the divergent oscillations shown in figures 7 and 8, the amplitudes of the oscillations increased to a maximum angle of attack of about 32° at a Mach number of 1.10. The amplitudes were damped to an angle of attack of about 23° at a Mach number of 0.9 and varied between 16° and 23° throughout the remaining decelerating portion of the flight. The variation with Mach number of the angular velocities in pitch and yaw during the oscillatory motions of the model is presented in figure 9.

The occurrence of high-amplitude oscillations at transonic speeds can be explained by the wind-tunnel results of references 4 and 5. These tests show that hysteresis loops were present in the pitching-moment curves as the result of separation and reattachment of the flow during the increasing and decreasing angle-of-attack cycles of the model. The energy imparted by the hysteresis loops produces the high-amplitude limit-cycle oscillations experienced by the model of this test. This phenomenon was also observed in the free-flight test data of reference 1. A point of interest in the data shown in figure 9 is the abrupt change in the periods and amplitudes of the angular velocities in pitch and yaw as the model decelerated through the transonic speeds. This type of motion indicates an abrupt rearward movement of the center of pressure at a Mach number of 0.98 with corresponding increases in the restoring and damping forces.

Base Pressures

The time history of the measured base pressure coefficients is included in figure 8 to show the variation of the base pressure coefficients during the oscillatory motions of the model at the transonic and subsonic speeds. Oscillations of the base pressure coefficient appeared to correspond to oscillations of the square of the resultant-force coefficient of the model. Figure 10 presents the variation of the base pressure coefficients with Mach number and shows that a large spread in the measured values of base pressure coefficients resulted from the high-amplitude oscillations of the model at Mach numbers below 1.25. Base pressure coefficients at approximately zero angle of attack were derived from the data of figures 10(a) and 10(b) by fairing values of the average base pressure coefficients at resultant-force coefficients corresponding to angles of attack of less than 2°. The variation of the average base pressure coefficients at approximately zero angle of attack with Mach number is presented in figure 10(c).

Drag

Measured values of the axial-force coefficients are presented as a function of Mach number in figure 11. These data also show a large

spread during the high-amplitude oscillations of the model at the transonic and subsonic speeds. Since the accuracy of the measured data decreases at the lower Mach numbers, the spread in the axial-force coefficients below a Mach number of 1.25 may be partly due to experimental errors. Measurements of the axial-force coefficients shown in figure 11 should therefore be used with caution at the lower Mach numbers. The total and base drag coefficients at approximately zero angle of attack are presented in figure 12 as a function of Mach number. The total drag coefficients were derived by fairing values of the axial-force coefficients at values of resultant-force coefficients corresponding to angles of attack of less than 2°. The base drag coefficients were computed from the average base pressure coefficients at approximately zero angle of attack.

The total drag coefficients for the model of this investigation (obtained from $C_{A,\alpha\approx 0}$ data) are compared in figure 12 with the total drag and base drag coefficients of the free-flight models of references 2 and 3 having the same nose shape. It should be noted that the drag coefficients of the models of references 2 and 3 are faired values for the oscillating model and are used qualitatively for substantiation of the total drag coefficients obtained for the present model at approximately zero angle of attack. Axial-force data at zero angle of attack for the wind-tunnel model of reference 4 are also presented in figure 12 for comparison with the total drag coefficients of the present model. The wind-tunnel model of reference 4 had the same nose shape as that of the present model. The total drag coefficients of the model of reference 2 agree fairly well with those of this investigation since the model of reference 2 experienced oscillations corresponding to angles of attack only of the order of 2° at the transonic speeds and from 4° to 5° at the subsonic speeds. The model of reference 3, however, experienced high-amplitude oscillations corresponding to angles of attack of the order of 10° to 20° and the total drag coefficients compare less favorably with the total drag coefficients of the present model at approximately zero angle of attack.

The differences shown between the total drag coefficients of the free-flight models in figure 12 do not reflect the differences in the base drag coefficients for these models. It is interesting to note that the variation of the base drag coefficients with Mach number of the present model is similar to that for the model of reference 3 and does not indicate the sharp decrease near a Mach number of 0.9 as shown for the model of reference 2.

Effect of Nose Shape

Figure 13 presents a comparison of the total drag coefficients at approximately zero angle of attack for the present model with those

for the free-flight models of reference 1 and the wind-tunnel models of reference 4. These data indicate that the increase in the total drag coefficient of the present model with a blunter nose shape than the models of reference 1 was approximately 0.2 at supersonic speeds. This increase agrees fairly well with the increment shown for the wind-tunnel models. Figure 14 presents a comparison of the base drag coefficients at approximately zero angle of attack for the present model with those for the two models of reference 1. The base drag coefficients of the models were approximately equal at Mach numbers above 1.25.

The differences noted in the total and base drag coefficients (figs. 13 and 14, respectively) near and below a Mach number of 1.0 indicate higher drag for the models with the less blunt nose. However, the increments in the drag coefficients for the two nose configurations at the transonic and subsonic speeds should be regarded only qualitatively since the test accuracy is lower below a Mach number of 1.0, and the Reynolds number effects on the separation and reattachment of the flow about such models may have a marked effect on the total and base drag of the models at these speeds. At speeds above a Mach number of approximately 1.2, however, the difference in the total drag coefficient at approximately zero angle of attack appears to be principally due to the difference in the drag of the nose of the models.

SUMMARY OF RESULTS

A free-flight investigation was conducted to determine the base pressures and drag of a flare-stabilized cylindrical reentry body with an elliptical blunt nose having a ratio of nose length to body radius of 0.29. The model was designed and tested to simulate the decelerating forces of a full-scale missile during the terminal phases of reentry. The center of gravity of the model was located at 42.7 percent of the body length and was flight tested over a Mach number range from 1.9 to 0.7. The Reynolds number range for the test was from 4.75×10^6 to 2.62×10^6, based on the body diameter. A summary of the results of this investigation is presented as follows:

1. The model experienced high-amplitude oscillations which began at a Mach number of 1.25 after a buildup in the resultant angle of attack to approximately 16°. While the model decelerated through a region of dynamic instability as indicated by the divergent oscillations, the maximum amplitude of the oscillations increased to an angle of attack of approximately 32° at a Mach number of 1.10. High-amplitude oscillations of approximately 16° to 23° were sustained throughout the remaining decelerating portion of the flight.

2. High-amplitude oscillations of the model at transonic and subsonic speeds resulted in a large spread in the measured values of the base pressure coefficients at Mach numbers below 1.25. In general, measured data indicated oscillatory values of the base pressure coefficient corresponding to oscillations of the square of the resultant-force coefficient of the model.

3. A large spread in the measured values of the axial-force coefficients was also obtained as a result of the high-amplitude oscillations of the model at the transonic and subsonic speeds. Comparison of the total drag coefficients with the results of other free-flight tests of similar models showed fairly good agreement as the oscillating models approached zero angle of attack.

4. A comparison of the present results with the results of free-flight tests of similar models with a less blunt nose having a ratio of nose length to body radius of 0.50 was made. This comparison indicated that the change in nose shape resulted in an increase in the total drag coefficient at approximately zero angle of attack of about 0.2 at supersonic speeds. The effect of nose bluntness on the base drag coefficients at approximately zero angle of attack appeared to be negligible at Mach numbers above 1.25.

Langley Research Center,
National Aeronautics and Space Administration,
Langley Field, Va., May 25, 1960.

REFERENCES

1. Mayhue, Robert J., and Blanchard, Willard S., Jr.: Free-Flight Investigation of the Base Pressure and Drag of a Flare-Stabilized Blunt-Nose Reentry Body Having a Fineness Ratio of 3.11 at Mach Numbers from 0.70 to 1.90. NASA TM X-214, 1960.

2. McFall, John C., Jr.: Drag Measurements of a Reentry Body With Rocket-Boosted Models in Free Flight at Mach Numbers From 2.8 to 0.6. NASA TM X-1, 1959.

3. McFall, John C., Jr.: Free-Flight Drag Measurements of Rocket-Boosted Models of Two Reentry Body Configurations at Mach Numbers From 4.3 to 0.6. NASA TM X-118, 1959.

4. Reese, David E., Jr., and Wehrend, William R., Jr.: An Investigation of the Static and Dynamic Aerodynamic Characteristics of a Series of Blunt-Nosed Cylinder-Flare Models at Mach Numbers From 0.65 to 2.20. NASA TM X-110, 1959.

5. Tunnell, Phillips J., Marker, Ralph D., and Reese, David E., Jr.: Characteristics of a Blunt-Nosed Cylindrical Flared Body in Pitch at Transonic Mach Numbers. NASA TM X-159, 1960.

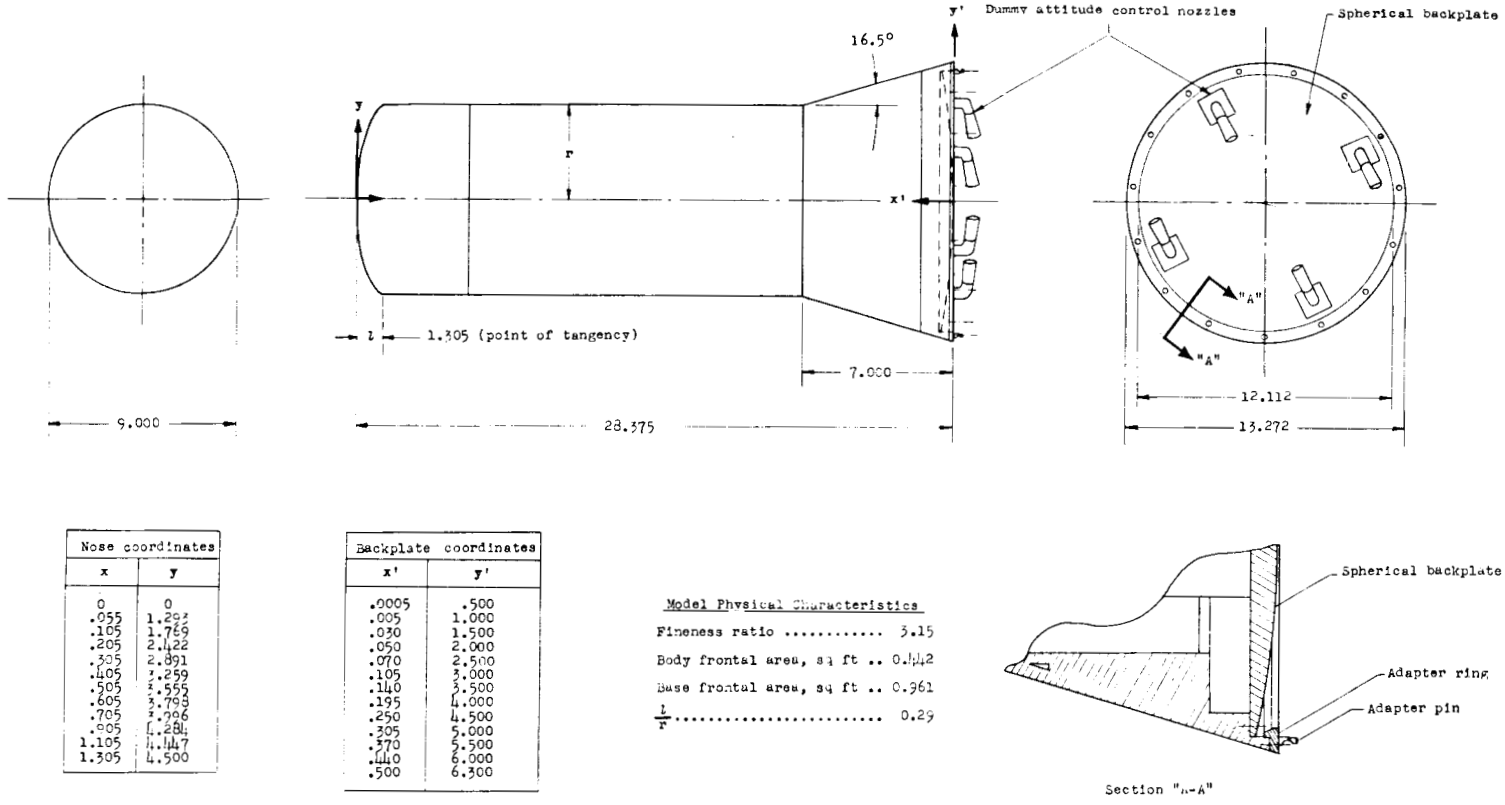

Nose coordinates	
x	y
0	0
.055	1.292
.105	1.769
.205	2.422
.305	2.891
.405	3.259
.505	3.555
.605	3.798
.705	3.996
.805	4.284
1.105	4.447
1.305	4.500

Backplate coordinates	
x'	y'
.0005	.500
.005	1.000
.030	1.500
.050	2.000
.070	2.500
.105	3.000
.140	3.500
.195	4.000
.250	4.500
.305	5.000
.370	5.500
.440	6.000
.500	6.300

Model Physical Characteristics

Fineness ratio 3.15

Body frontal area, sq ft .. 0.442

Base frontal area, sq ft .. 0.961

$\frac{l}{r}$ 0.29

Figure 1.- Model dimensions and physical characteristics. All dimensions are in inches.

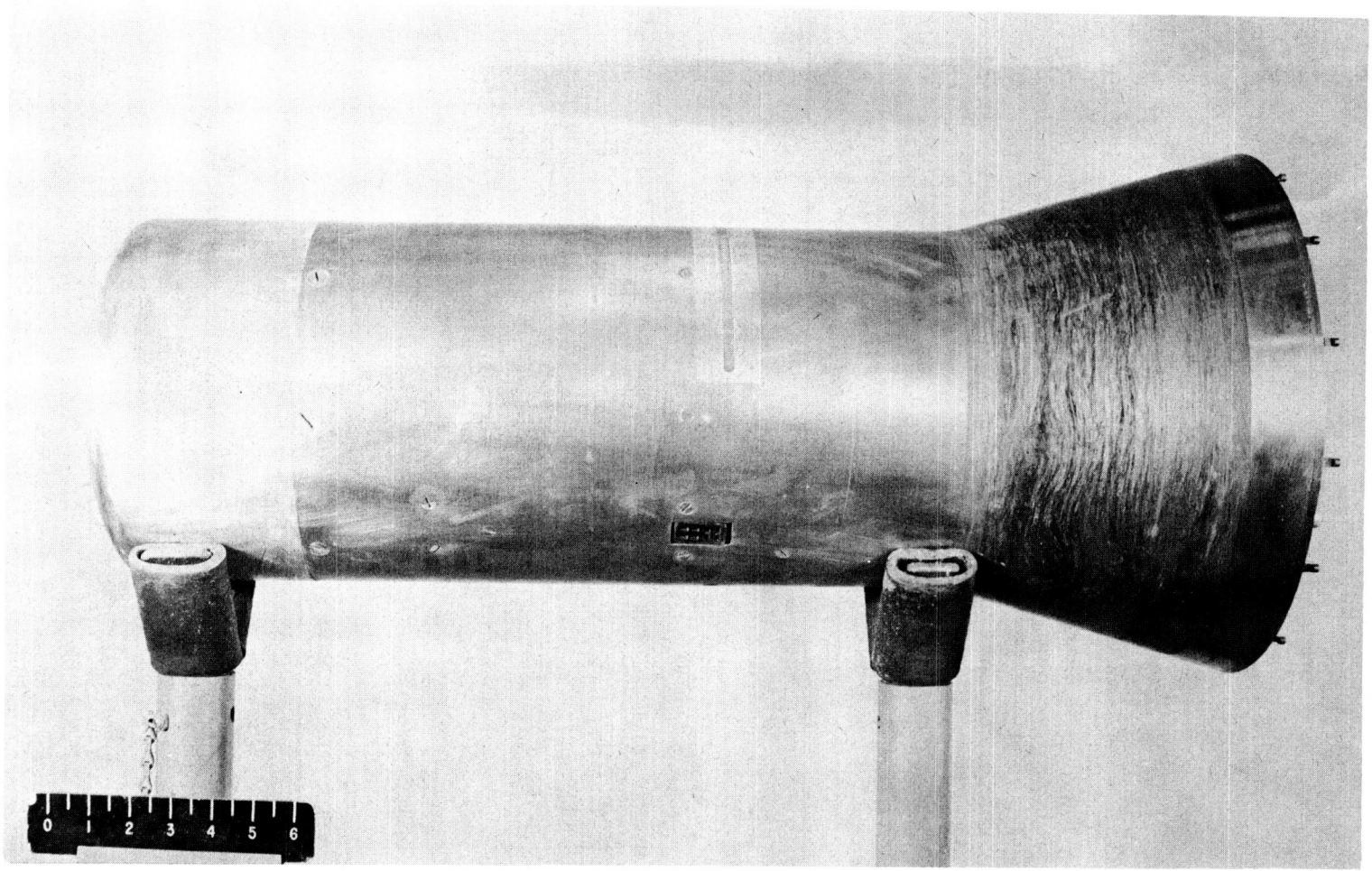

Figure 2.- Photograph of model tested. L-58-4282

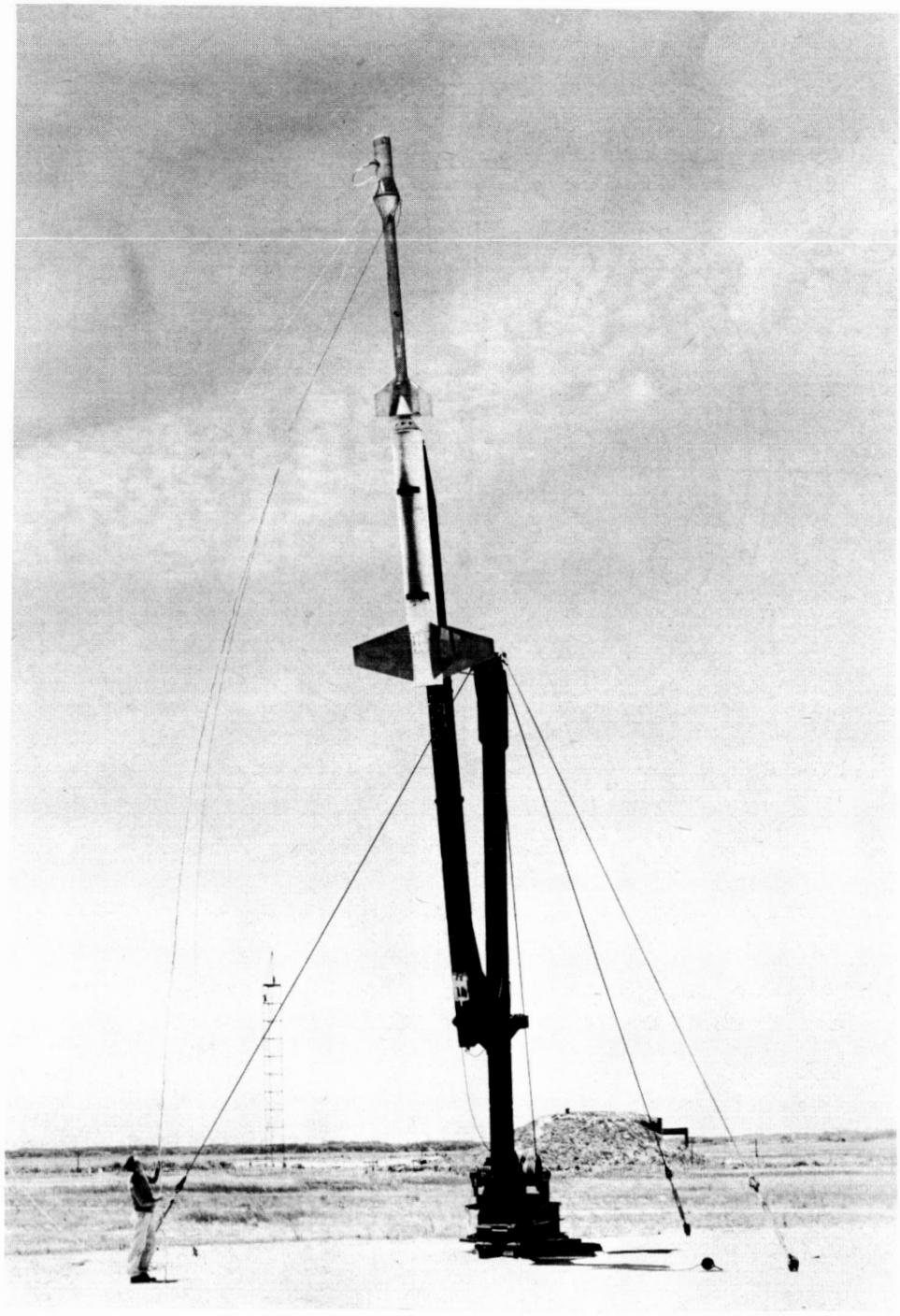

L-58-2658

Figure 3.- Photograph of model and booster in launching position.

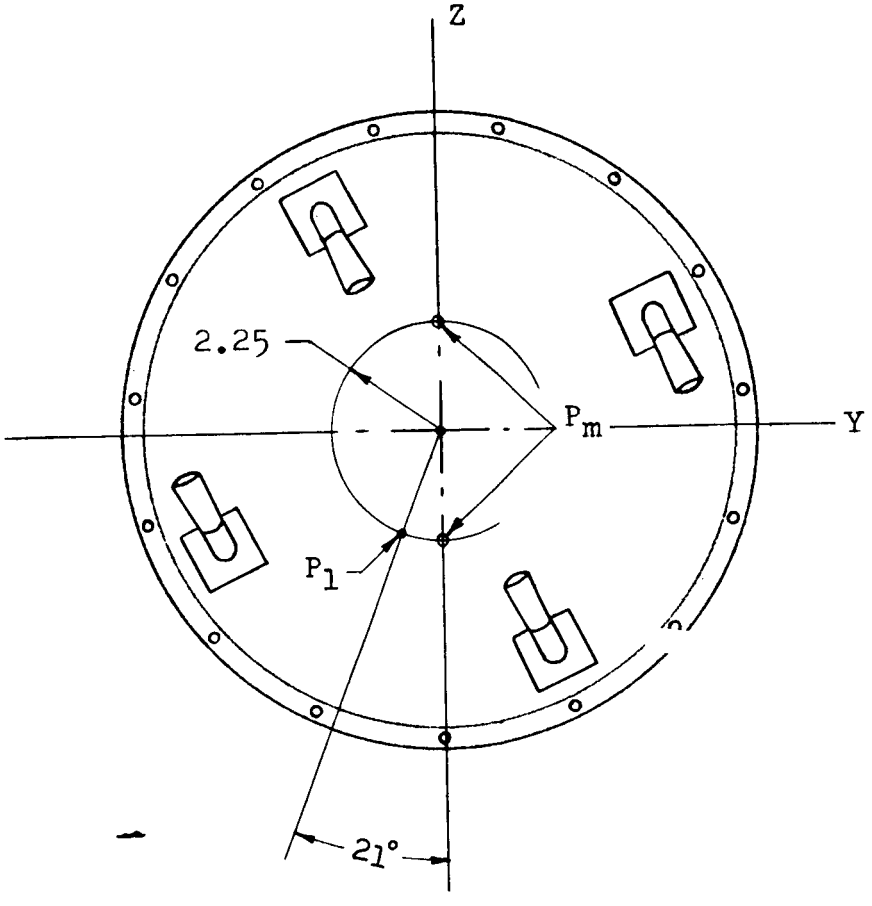

Orifice Size

P_m = 0.180 I.D.

P_1 = 0.055 I.D.

Figure 4.- Location of base pressure orifices. All dimensions are in inches.

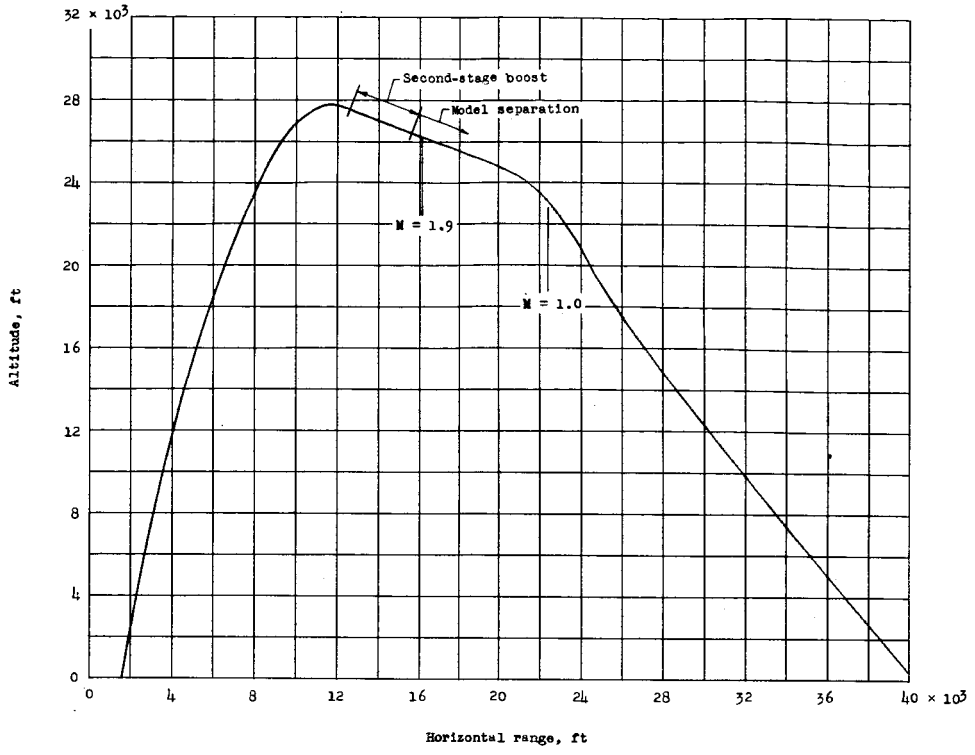

(a) Flight-test trajectory.

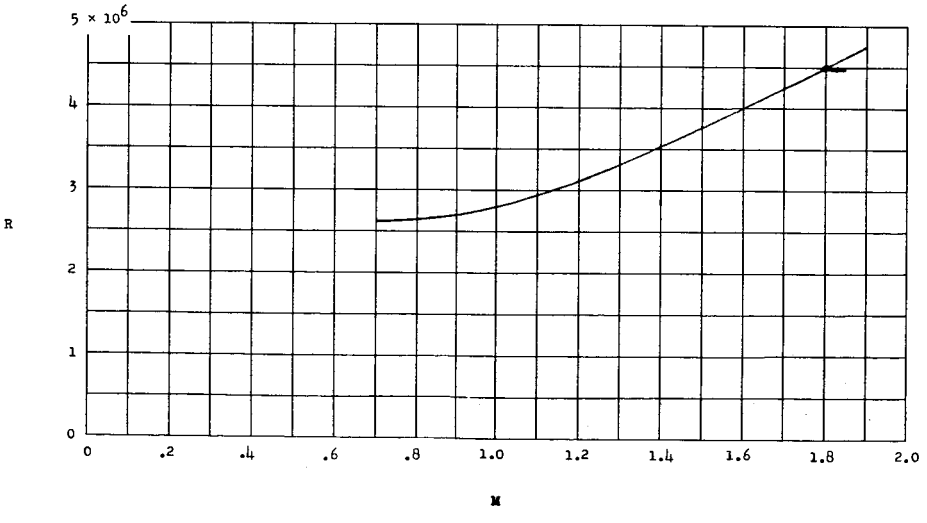

(b) Flight-test Reynolds number.

Figure 5.- Flight-test trajectory and variation of flight-test Reynolds number with Mach number.

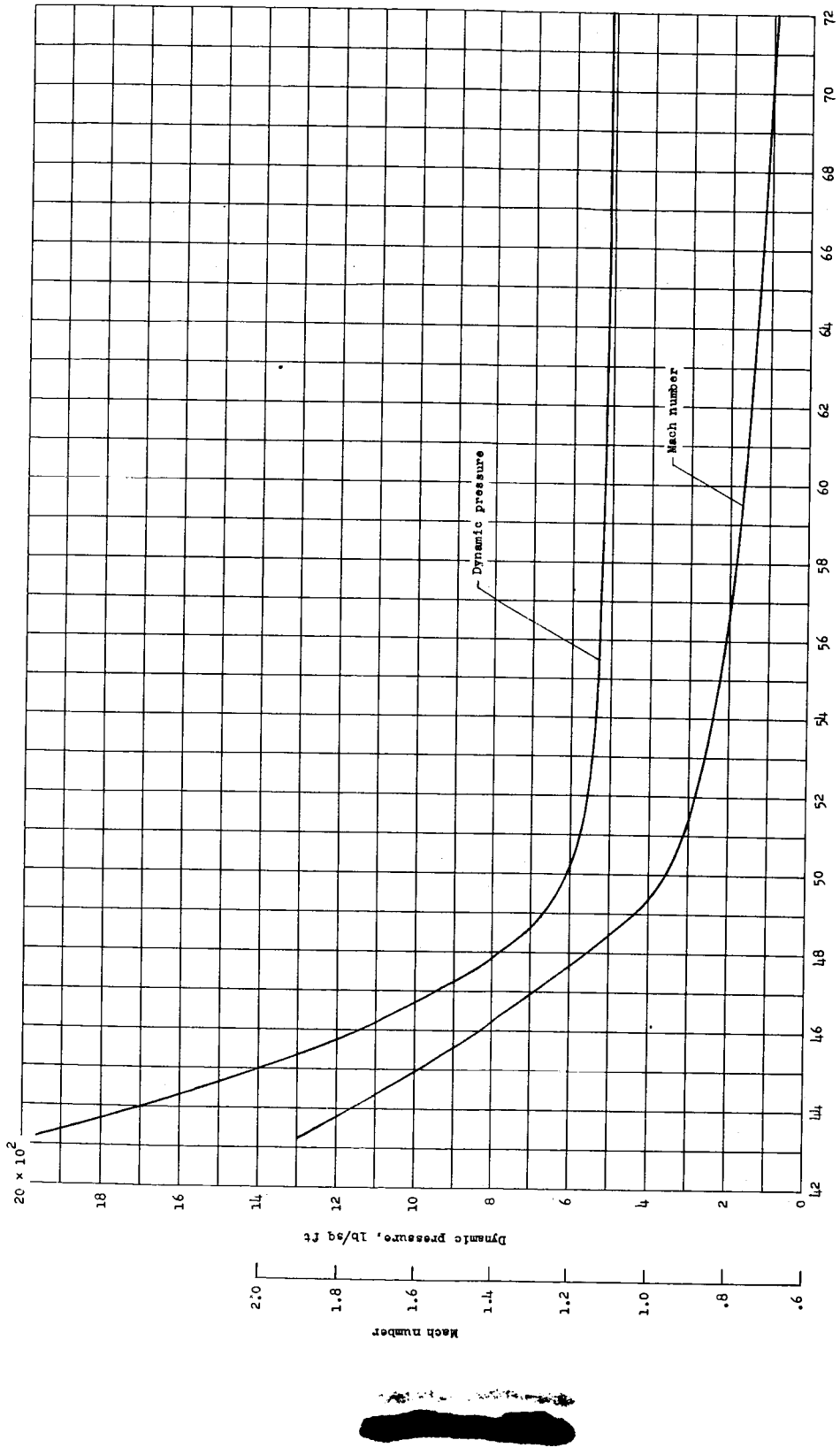

Figure 6.- Time history of the flight-test dynamic pressure and Mach number.

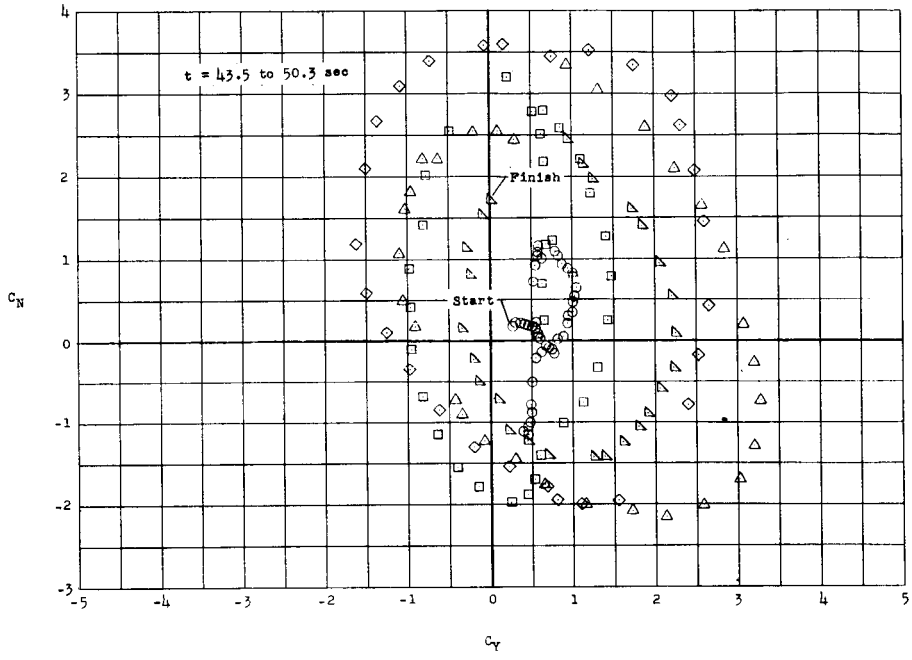

(a) M = 1.86 to 0.94.

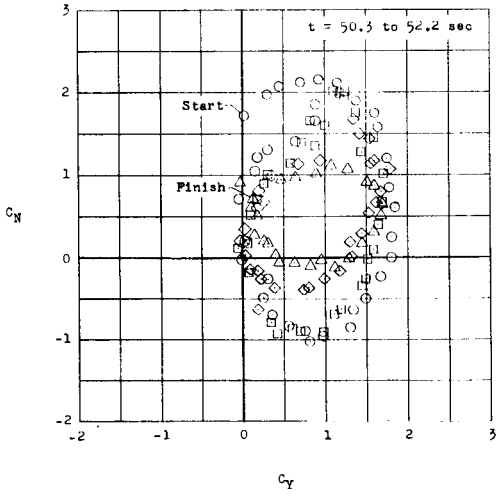

(b) M = 0.94 to 0.88.

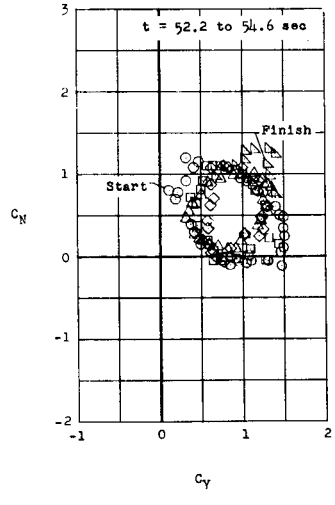

(c) M = 0.88 to 0.83.

Figure 7.- Variation of normal-force coefficient with transverse-force coefficient from Mach number 1.86 to 0.83. Increasing time is indicated by the symbols ○ □ ◇ △ ◺.

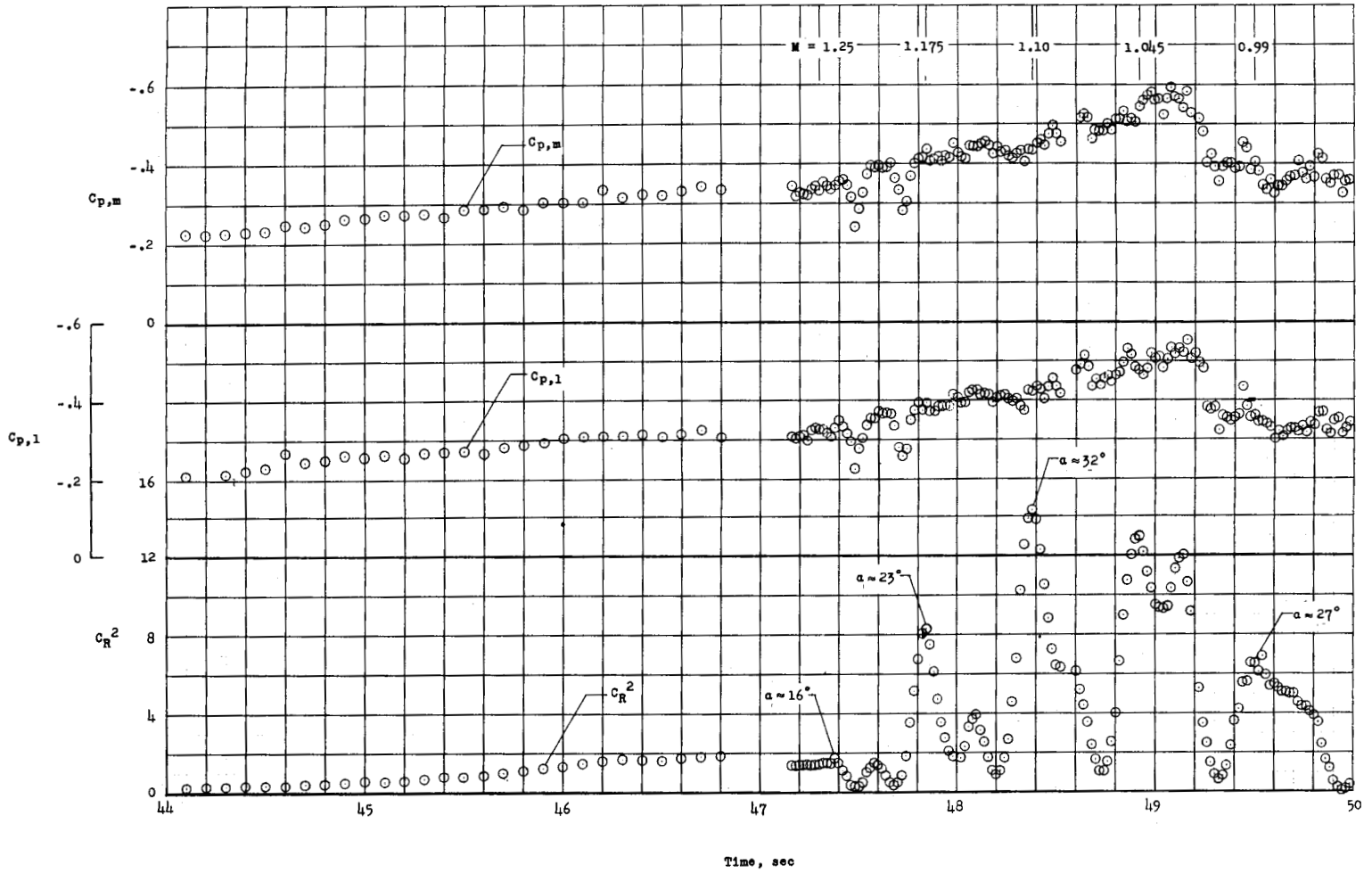

(a) t = 44 to 50 seconds.

Figure 8.- Time history of base pressure coefficients and square of resultant-force coefficients.

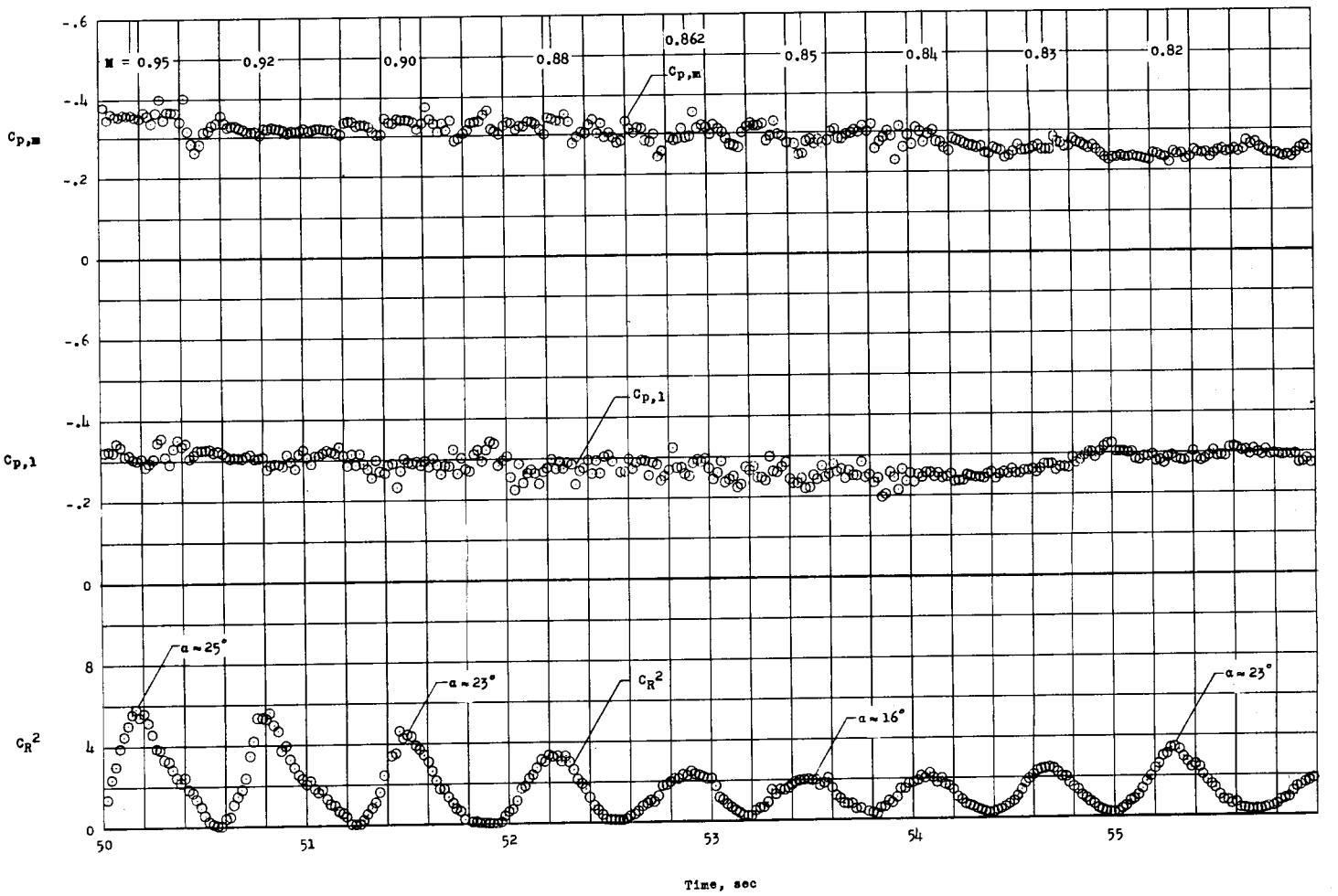

(b) t = 50 to 56 seconds.

Figure 8.- Continued.

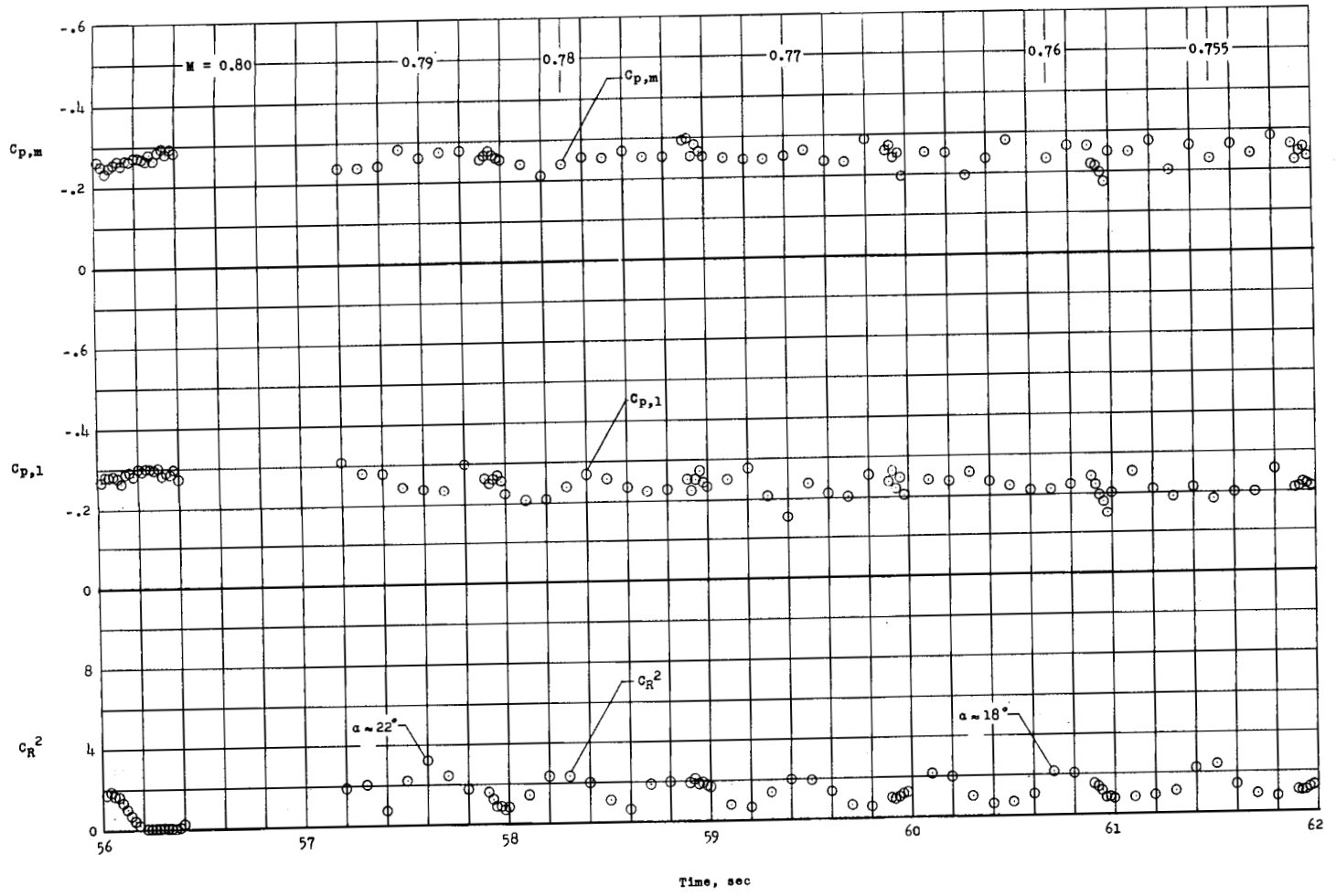

(c) t = 56 to 62 seconds.

Figure 8.- Continued.

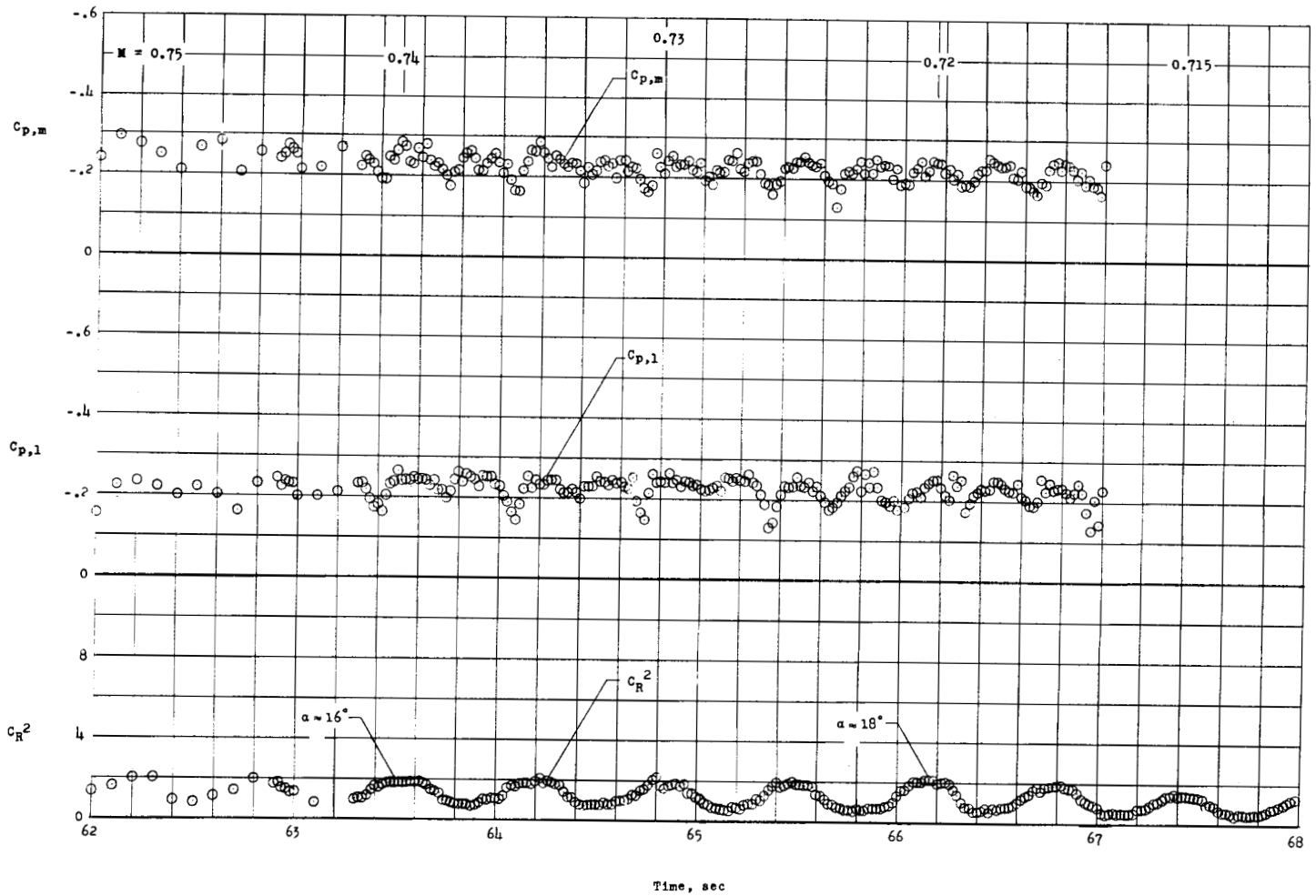

(d) t = 62 to 68 seconds.

Figure 8.- Concluded.

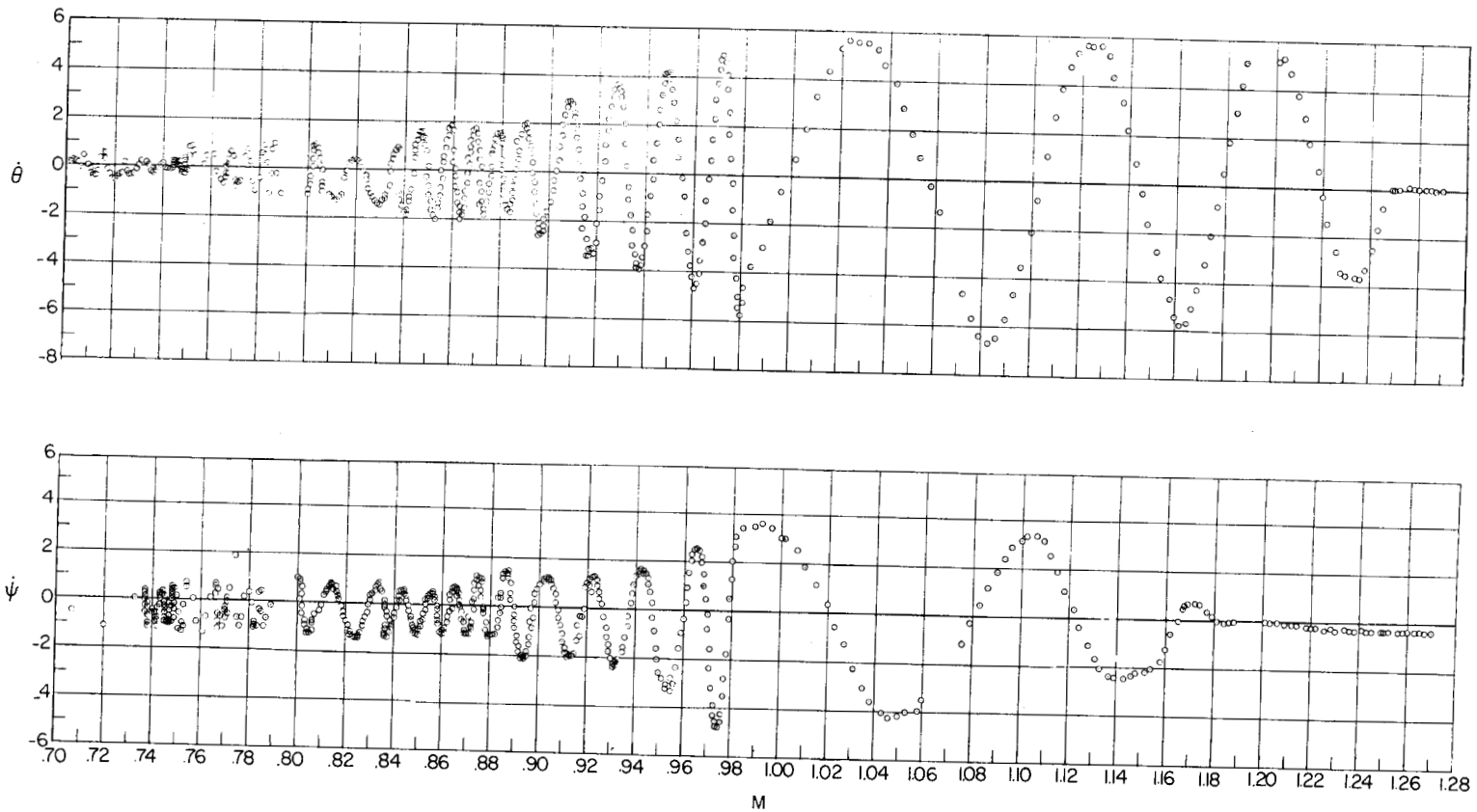

Figure 9.- Variation with Mach number of angular velocities in pitch and yaw.

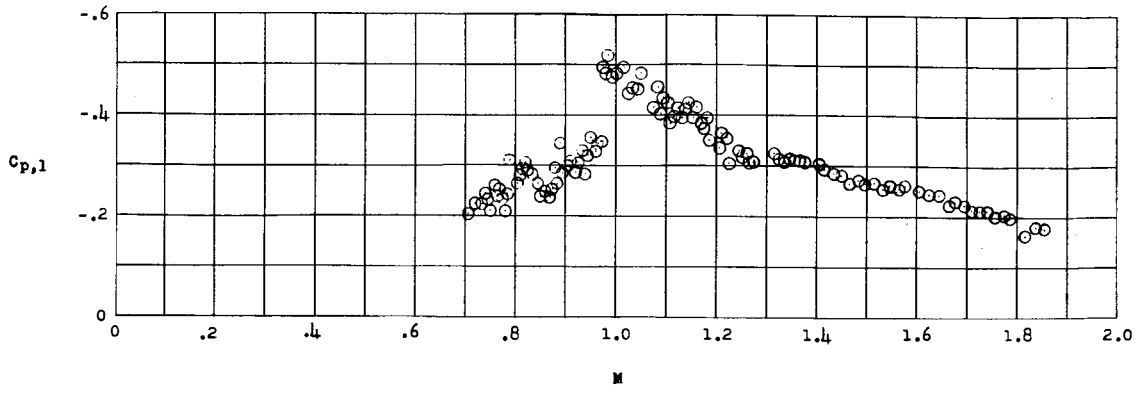

(a) Pressure coefficient at station 1.

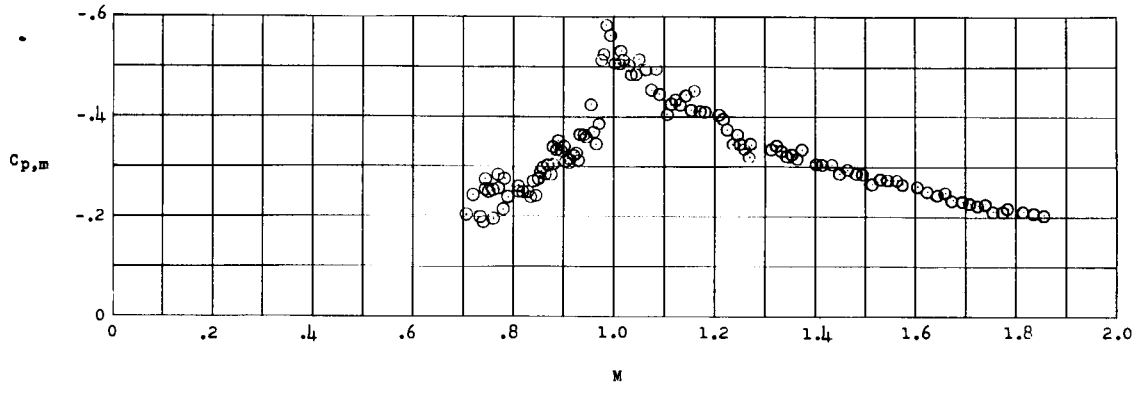

(b) Manifold pressure coefficient.

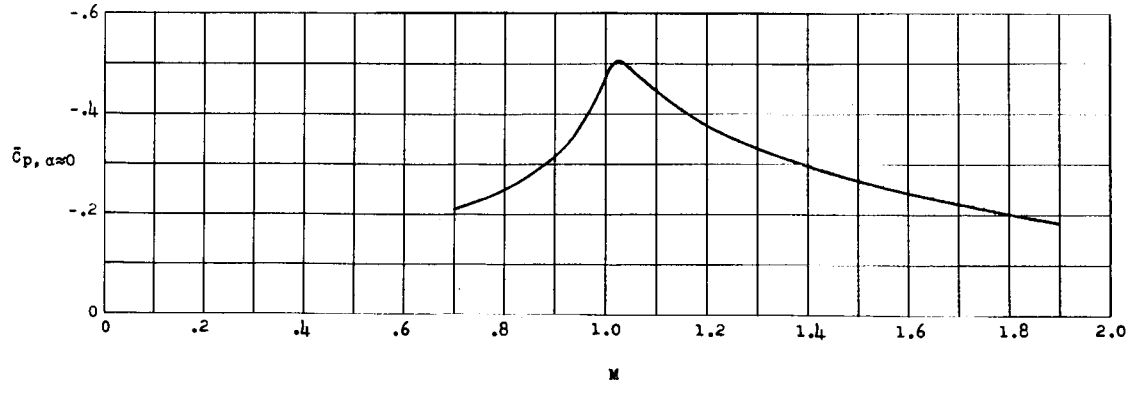

(c) Average pressure coefficient at approximately zero angle of attack.

Figure 10.- Variation of base pressure coefficients with Mach number.

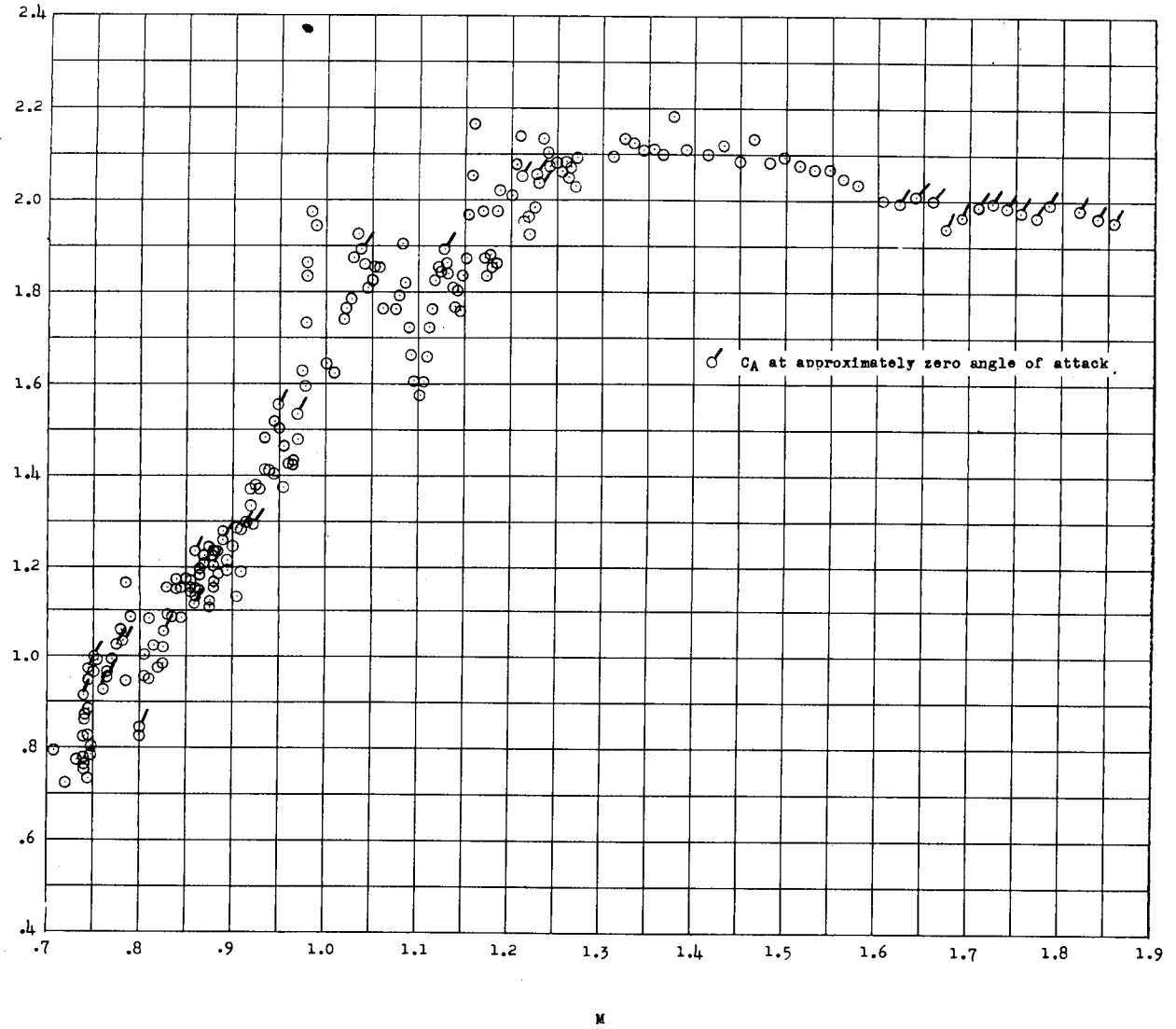

Figure 11.- Variation of axial-force coefficient with Mach number.

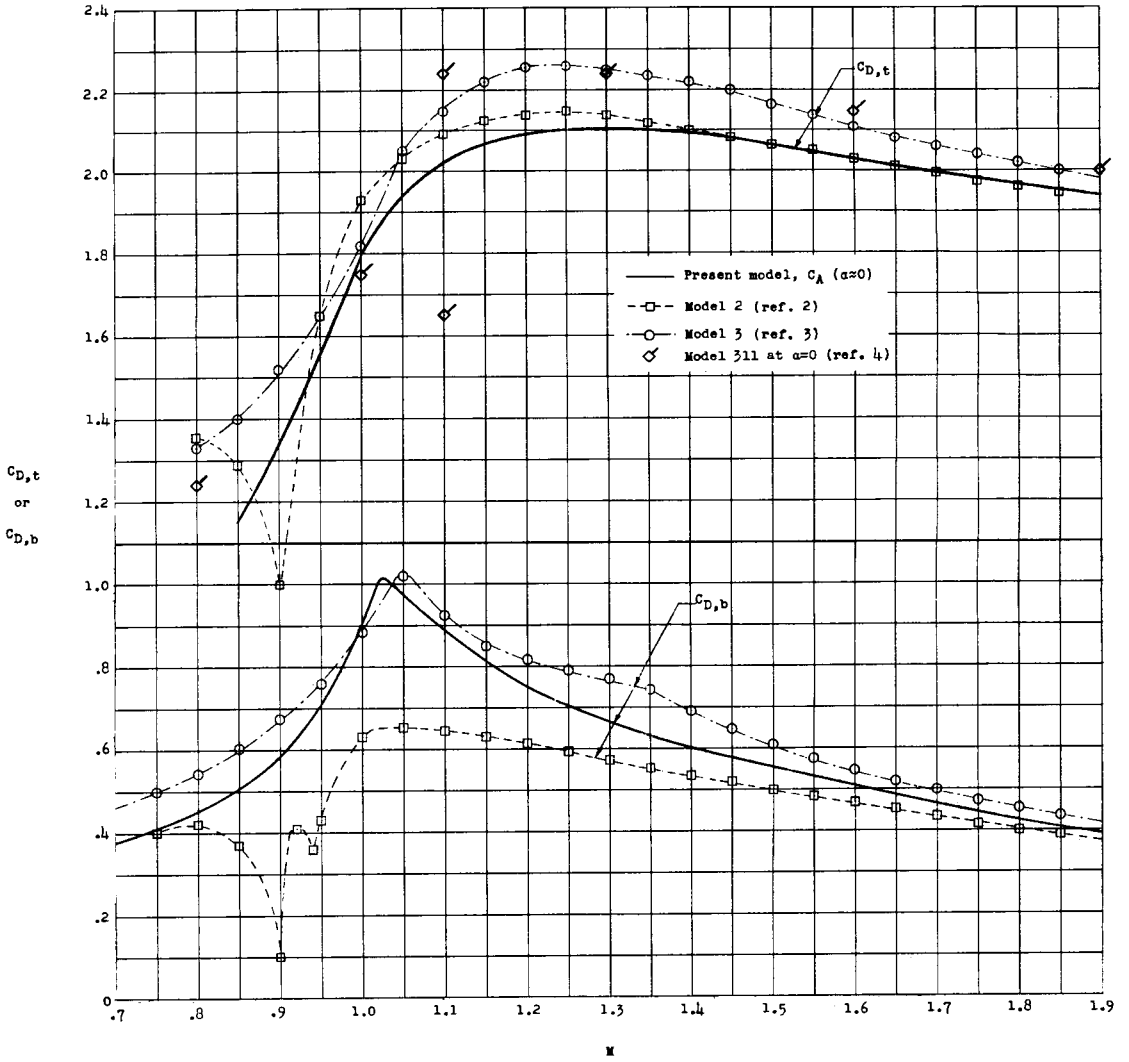

Figure 12.- Variation of the total and base drag coefficients with Mach number.

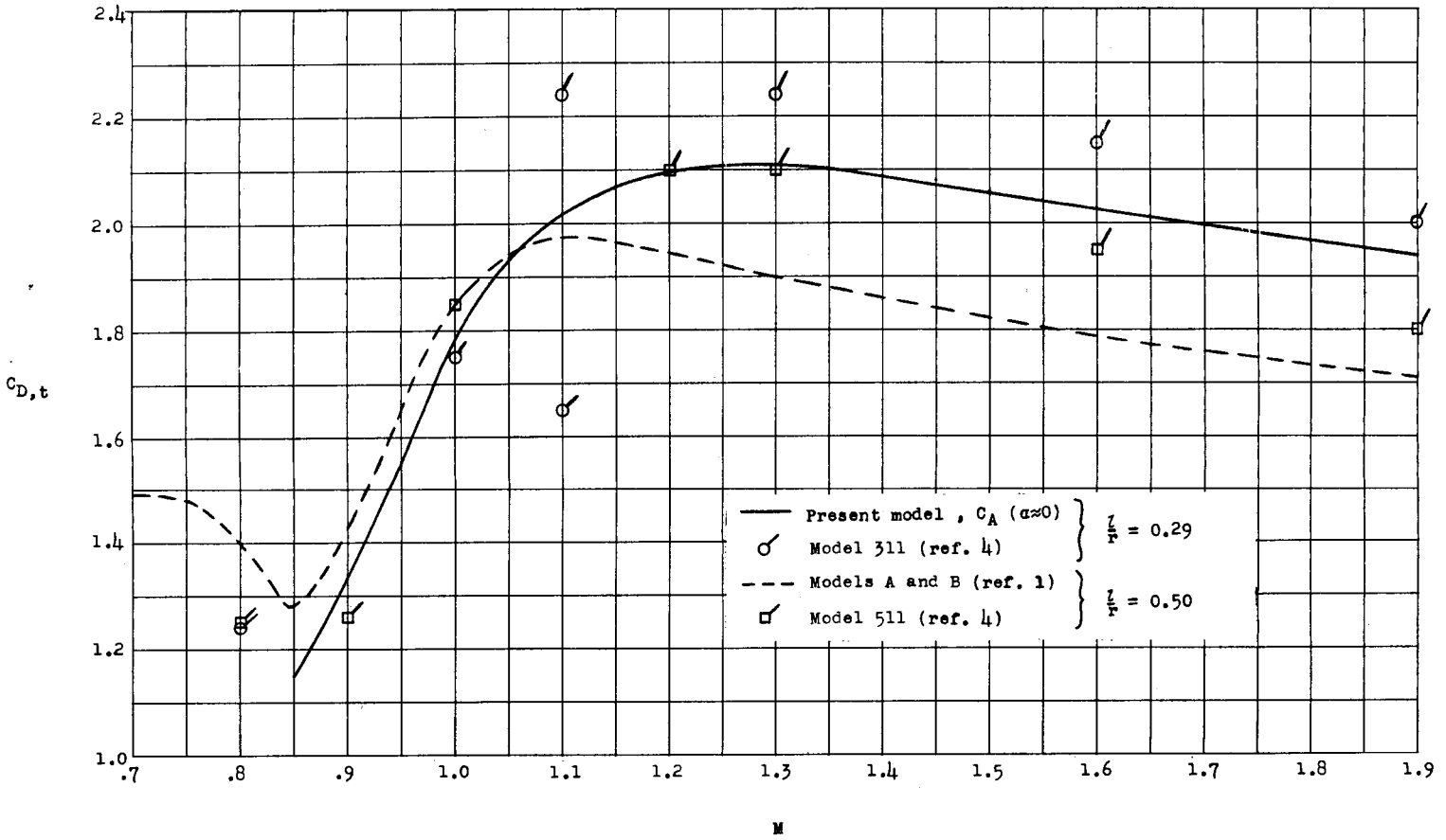

Figure 13.- Effect of nose shape on the total drag coefficient at approximately zero angle of attack.

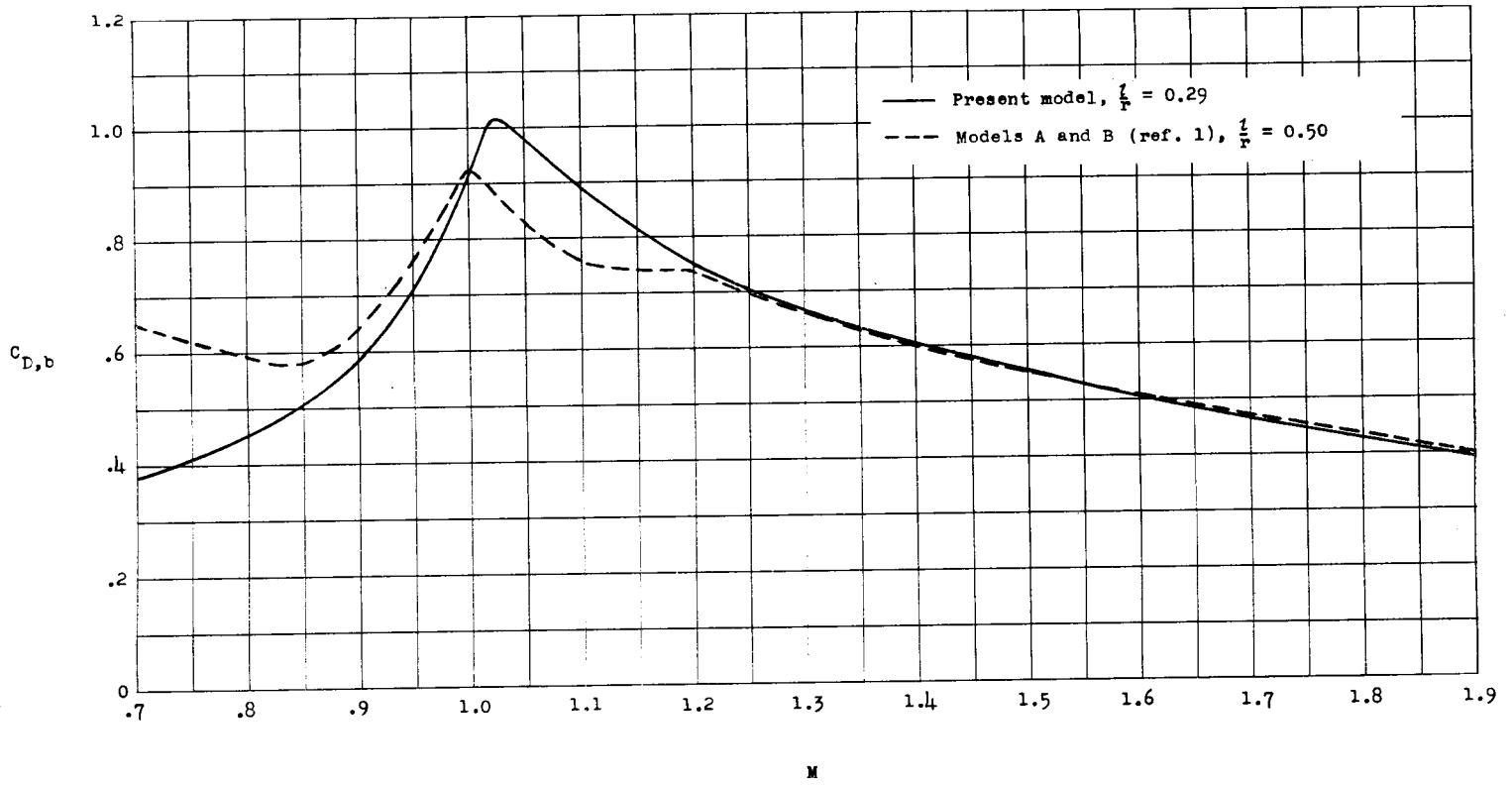

Figure 14.- Effect of nose shape on the base drag coefficient at approximately zero angle of attack.